Catalysis Today 149 (2010) 62–68

Contents lists available at ScienceDirect

Catalysis Today

journal homepage: www.elsevier.com/locate/cattod

Preparation, characterization and hydrotreating performances of ZrO_2–Al_2O_3-supported NiMo catalysts

Dengqian Zhang [a], Aijun Duan [a,*], Zhen Zhao [a,*], Guofu Wan [a], Zhenyong Gao [a], Guiyuan Jiang [a], Kebin Chi [b], Keng H. Chuang [c]

[a] State Key Laboratory of Heavy Oil Processing, China University of Petroleum, Beijing 102249, PR China
[b] Research Center of Daqing Chemical Engineering, Petrochina Corporation Limited, Daqing 163714, PR China
[c] Department of Chemical and Petroleum Engineering, University of Calagary, Calagary, T2N 1N4 Canada

ARTICLE INFO

Article history:
Available online 2 June 2009

Keywords:
Al_2O_3–ZrO_2 composite
Hydrodesulfurization
Hydrodenitrogenation
Catalyst
Diesel oil

ABSTRACT

A series of Al_2O_3–ZrO_2 composite supported NiMo catalysts with various ZrO_2 contents were prepared. Several techniques including XRD, SEM, N_2 physisorption, H_2-TPR, and UV–vis DRS were used for typical physico-chemical properties characterization of the ZrO_2–Al_2O_3 composite supports and their NiMo/ZrO_2–Al_2O_3 catalysts. The test results showed that the composite supports prepared by the chemical precipitation method existed as amorphous phase in the samples with insufficient contents of ZrO_2, and the incorporation of ZrO_2 into supports provided a better dispersion of NiMo species, which made their reductions become easier. The pyridine-adsorbed FT-IR results indicated that the Lewis acid sites of catalysts increased significantly by the introduction of ZrO_2 into the supports. The activities of these catalysts for diesel oil hydrodesulfurization (HDS) and hydrodenitrogenation (HDN) were evaluated in a high pressure micro-reactor system. The results showed that the ZrO_2–Al_2O_3-supported NiMo catalysts with suitable ZrO_2 contents exhibited much higher catalytic activities than that of Al_2O_3-supported one, and when the ZrO_2 contents were 15% and 5%, the NiMo/Al_2O_3–ZrO_2 catalysts presented the highest HDS and HDN activities, respectively.

1. Introduction

The stringent environmental regulations promoted the establishment of the rigorous specifications of high quality transportation fuels. The Tier II regulations from US Environmental Protection Agency required that on-road diesel oil's sulfur specification was lowered to 15 ppmw after June 2006, and the EU specification was expected to be below 50 ppmw in 2005 and will be about 10 ppmw around 2010 [1,2]. The traditional hydrotreating process is one of the important techniques to remove the sulfur and nitrogen heteroatom compounds for producing the clean transportation fuels, however, it would be more difficult to obtain the ultra low sulfur fuels depending on the existed common hydrotreating techniques. The challenges in producing ultra clean fuels in an economically affordable manner drive the researchers in the world to develop new technologies including catalysts, processes, and reactors. Thus, the development and application of more active and better performance hydrotreating catalysts are, among all the technologies, the most desired approaches to enhance the product quality.

Traditional hydrotreating catalysts are alumina-supported Mo or W sulfides promoted by Ni or Co. As an important component of hydrotreating catalysts, the support has a direct interaction with the active metal species, and has an indirect role in determining the promotional effects of the secondary metal species [3,4]. A favorable support should provide the suitable structure and the profitable physico-chemical property. A mixed support might be a good choice, since a suitable mixture may offer a combination of the desirable properties of each component [5–7]. For example, as the typical oxides, TiO_2 and ZrO_2 possess good redox properties and exhibit the promising HDS activities [7,8], but their low thermal stability and low surface areas have prevented their wide applications as the unique support in the industrial HDS catalysts [9]. To overcome those disadvantages, many studies were carried out concerning the mixed oxide supports, for example, TiO_2–Al_2O_3, ZrO_2–Al_2O_3 [7–11], etc. Research showed that the combination of TiO_2 and Al_2O_3 lead to the increased reducibility and sulfurability of Ni(Co)Mo catalysts, which was related to the fact that the redox processes of the active phases (Mo) were facilitated by the

* Corresponding authors. Tel.: +86 10 89731586.
E-mail addresses: duanaijun@cup.edu.cn (A. Duan), zhenzhao@cup.edu.cn (Z. Zhao).

0920-5861/$ – see front matter © 2009 Elsevier B.V. All rights reserved.
doi:10.1016/j.cattod.2009.04.012

semiconductor character of TiO_2 compared with the pure insulating Al_2O_3 [10,11]. The modification of the surface of alumina with TiO_2 eliminated the most of reactive surface hydroxyl groups and avoided the formation of tetrahedral Mo oxide species, resulting in an increase of octahedral Mo active species and thus leading to a higher HDS activity [12,13].

Recently, more and more considerations are taken into account the use of ZrO_2–Al_2O_3 mixed oxides as HDS catalytic supports due to the unique properties of ZrO_2, i.e., to simultaneously sustain acidic and basic sites and to possess good redox properties [14,15]. Li et al. [16,17] prepared ZrO_2–Al_2O_3 composite oxides by precipitation of $ZrOCl_2{\cdot}8H_2O$ and pseudo-boehmite, and they also investigated the HDS performance of dibenzothiophene (DBT) on the sulfided CoMo/ZrO_2–Al_2O_3 catalysts. The results showed that CoMo/ZrO_2–Al_2O_3 catalyst with suitable ZrO_2 content (12.1 wt%) in supports had a higher activity for HDS of DBT than CoMo/Al_2O_3. ZrO_2–Al_2O_3 composite oxides were also prepared by impregnating alumina with a solution of zirconium n-propoxide, and the corresponding Mo/ZrO_2–Al_2O_3 catalysts showed the higher thiophene HDS activity than Mo/Al_2O_3 [9]. However, unlike TiO_2–Al_2O_3 system that has been studied extensively and thoroughly for its brightening prospects in industry [7,8,18–20], the preparation and the properties of ZrO_2–Al_2O_3 as a kind of new catalyst support materials have not been sufficiently studied yet, especially for hydrotreating of real diesel oil feedstocks.

In the present work, a series of ZrO_2–Al_2O_3 composite oxides with various ZrO_2 contents were prepared by deposition of $ZrOCl_2{\cdot}8H_2O$ on alumina, and the synthesized ZrO_2–Al_2O_3 samples were purposively used as the supports for NiMo hydrodesulfurization (HDS) and hydrodenitrogenation (HDN) catalysts. An investigation was carried out to study the effect of ZrO_2 contents in ZrO_2–Al_2O_3 composites on HDS and HDN performances of NiMo/ZrO_2–Al_2O_3 series catalysts with diesel oil feedstock.

2. Experimental

2.1. Preparation of ZrO_2–Al_2O_3 composite oxides

The series of ZrO_2–Al_2O_3 composite oxides was designated as AZ*x*, where *x* represented the weight percentage of ZrO_2 based on ZrO_2–Al_2O_3. The preparation of AZ*x* composite oxides employed the following procedures: pseudo-boehmite and deionized water were mixed with vigorous stirring, and then $ZrOCl_2{\cdot}8H_2O$ aqueous solution with the concentration of 0.5 mol L^{-1} was dripped into the above system at a speed of 5 mL min^{-1}. As the liquid system became homogeneous, ammonia solution was slowly added into the liquid mixture until the final pH equalled to 7–8. The mixture was aged for 4 h at room temperature, and then dispersed in an ultra-sonic unit for 20 min. The obtained solid was thoroughly washed with deionized water until no chloride ion could be detected with $AgNO_3$ solution in the filtrate, and then the residue solid was washed with ethanol for three times. After that, the solid was dried in atmosphere overnight at 120 °C. Finally, the dried solid was calcined at 550 °C for 4 h in air.

2.2. Catalysts preparation

The corresponding NiMo/ZrO_2–Al_2O_3 series of catalysts were obtained by the two-step incipient-wetness impregnation method using ammonium heptamolybdate and nickel nitrate. After each impregnation step, the samples were dried at 110 °C for 12 h, and calcined at 550 °C for 4 h. All the samples were prepared with the constant amounts of Mo and Ni (corresponding to MoO_3 15.5 wt%, NiO 3.5 wt%).

2.3. Catalyst characterization

The composite supports and the catalysts were characterized by XRD, SEM, N_2 physisorption, H_2-TPR, and UV–vis DRS, etc. Scan electron microscope (SEM) studies were performed using a Cambridge S-360 apparatus. X-ray powder diffraction (XRD) profiles were recorded in an XRD-6000 diffractometer using Cu Kα radiation under 40 kV, 30 mA, scan range from 20° to 80° at a rate of 4° min^{-1}. The UV–vis diffuse reflectance spectra (DRS) experiments were performed on Hitachi U-4100 UV-Vis spectrophotometer with the integration sphere diffuse reflectance attachment. The powder samples were loaded in a transparent quartz cell and were measured in the region of 200–800 nm at room temperature. Porosity and surface area measurements of samples were performed on a Micromeritics ASAP 2020 automated gas adsorption system. All the samples were degassed at 400 °C under vacuum prior to N_2 adsorption at −196 °C. H_2-TPR was carried out using 10% hydrogen in helium at a constant flow rate of 40 mL min^{-1}, from 100 to 1000 °C, at a heating rate of 10 °C min^{-1}. The nature of acid sites of the catalysts was determined by pyridine-adsorbed Fourier transformed infrared (Pyridine FT-IR) spectroscopy on a MAGNAIR 560 FTIR instrument (Nicolet Co., America) with a resolution of 1 cm^{-1}. The samples were dehydrated at 500 °C for 5 h under a vacuum of 1.33×10^{-3} Pa, followed by the adsorption of purified pyridine vapor at room temperature for 20 min. Then, the system was evacuated at different temperatures and the pyridine-adsorbed IR spectra were recorded.

2.4. Catalytic activity measurement

The feedstock used in this paper was Daqing FCC diesel oil with 1810 ppm S and 1288 ppm N. The properties of the diesel oil feedstock are shown in Table 1. Catalytic performances were evaluated in a high-pressure fixed-bed reactor with 2 g of catalyst (grain size of 0.3–0.5 mm). All catalysts were presulfided for 4 h with a 2 m% CS_2–cyclohexane mixture under the conditions of LHSV (Liquid Hourly Space Velocity) of 1.0 h^{-1}, temperature of 320 °C, total pressure of 4 MPa and an H_2/cyclohexane ratio of 600 mL mL^{-1}. Hydrodesulfurization and hydrodenitrogenation tests were carried out under the conditions of 350 °C, 5.0 MPa, H_2/oil ratio of 600 mL mL^{-1} and LHSV of 1.0 h^{-1}. Catalytic activities were measured at steady state after 13 h on-stream. The catalytic activities under investigation were estimated by HDS and HDN efficiencies.

Table 1
The typical physico-chemical properties of diesel feedstock.

Properties	Data
Source	Daqing FCC
Sulfur (μg g^{-1})	1810
Nitrogen (μg g^{-1})	1288
Distillation (°C)	
IBP	181
5%	217
10%	223
20%	239
30%	251
40%	262
50%	278
60%	294
70%	312
80%	332
90%	351
95%	362

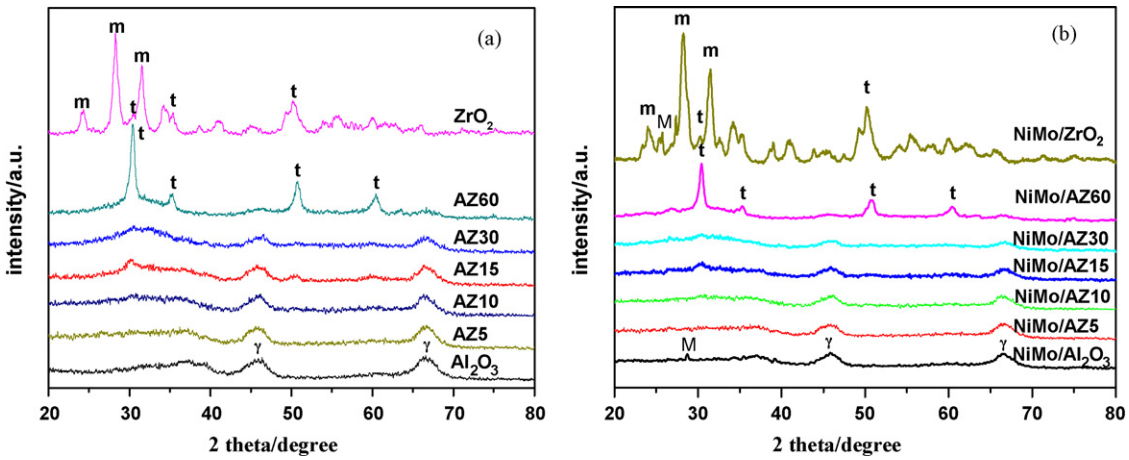

Fig. 1. The XRD patterns of the samples: (a) AZ*x* composites and (b) NiMo/AZ*x* catalysts. *Note*: (m) Monoclinic ZrO_2; (t) tetragonal ZrO_2; (γ) γ-Al_2O_3; and (M) MoO_3.

3. Results and discussion

3.1. XRD analysis

The XRD patterns of the AZ*x* series of composites and NiMo/AZ*x* series of catalysts are shown in Fig. 1(a) and (b), respectively. From Fig. 1(a), it can be seen that the Al_2O_3 obtained by calcination of pseudo-boehmite at 550 °C presented as the typical structure of γ-Al_2O_3. Compared with Al_2O_3 support, the composite supports AZ5 and AZ10 showed no other peak, indicating that low content of ZrO_2 in the composite supports existed as amorphous phase. With the increasing of the ZrO_2 contents, the binary oxide samples of AZ15 and AZ30 showed a weak intensity peak at $2\theta = \sim 30°$, which was attributed to the tetragonal ZrO_2. However, the XRD pattern of AZ60 showed two sharp peaks at $2\theta = 30.4°$ and 50.4°, which were obviously the characteristics of the tetragonal ZrO_2. No typical peak ascribed to the monoclinic ZrO_2 ($2\theta = 28.2°$ and 31.52°) [16,21] was observed in the pattern of AZ60, namely, ZrO_2 component in AZ60 binary composites was only existed as the tetragonal phase or might contain a small amount of monoclinic phase that was beyond the detection limit of the XRD method. On the other hand, the pattern of the pure ZrO_2 revealed that the sample was chiefly composed of monoclinic zirconia, and also with a small quantity of tetragonal zirconia. These results showed that the metastable tetragonal ZrO_2 was more stable at room temperature owing to the incorporation of Al_2O_3. This might be due to the homogenous dispersion of alumina and zirconia with each other. The incorporation of ZrO_2 into Al_2O_3 apparently prevented the aggregation of ZrO_2 nano-particles, and made the binary oxides of ZrO_2–Al_2O_3 existing as high dispersed smaller particles, which were propitious for the stabilization of the metastable tetragonal ZrO_2 [16,22]. In order to investigate the formation and stability of the tetragonal ZrO_2 in the AZ*x* composites furtherly, AZ15 support was calcined at 400, 550 and 800 °C, and the crystal information was also obtained by XRD (as seen in Fig. 2). In the AZ15 support the characteristic peaks of the tetragonal ZrO_2 appeared at the calcination temperature of 550 °C, and sustained until the temperature of 800 °C. In all the samples, the intensities of the peaks at $2\theta = 45°$ and 66°, which were attributed to γ-Al_2O_3, decreased with the increasing contents of ZrO_2. As shown in Fig. 1(b), the weak diffraction peaks at $2\theta = 25.7°$ and 28.7°, which attributed to the bulk MoO_3 phase and $NiMoO_4$ phase, respectively, were detected in the samples of NiMo/ZrO_2 and NiMo/Al_2O_3. However, no characteristic peak of bulk active metal oxides was detected in the other catalysts, indicating that the composite supports were beneficial to the dispersion of the active metals.

3.2. SEM characterization

SEM was used to observe the morphology of the oxide samples. The images of Al_2O_3 and AZ15 are shown in Fig. 3. It can be seen from Fig. 3 that the Al_2O_3 presented as large blocks with the sizes of 2–5 μm aggregated by the flocculent fiber, while AZ15 appeared as smaller spherical particles with the sizes of 300–500 nm. This indicated that the introduction of ZrO_2 into Al_2O_3 largely changed the morphology of the support composites. The morphology change from large blocks into small particles resulted in the formation of more interpores between the small particles. This was also confirmed by the N_2 adsorption results.

3.3. N_2 adsorption

The N_2 adsorption–desorption isotherms of NiMo/AZ*x* catalysts are shown in Fig. 4. The pore structural parameters (specific surface area, cumulative pore volume and average pore diameter) determined from the N_2 adsorption–desorption isotherms are listed in Table 2. All the NiMo/AZ*x* catalysts exhibited the typical type IV isotherms according to BDDT classification, as expected for

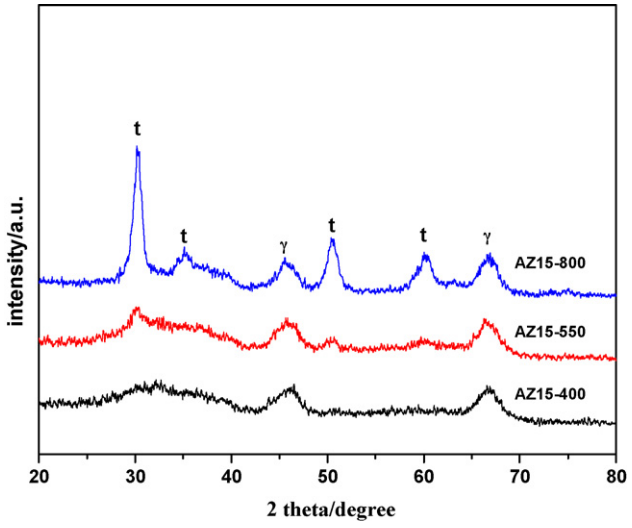

Fig. 2. The XRD patterns of the AZ15 composites calcined at 400, 550 and 800 °C. *Note*: (m) Monoclinic ZrO_2; (t) tetragonal ZrO_2; and (γ) γ-Al_2O_3.

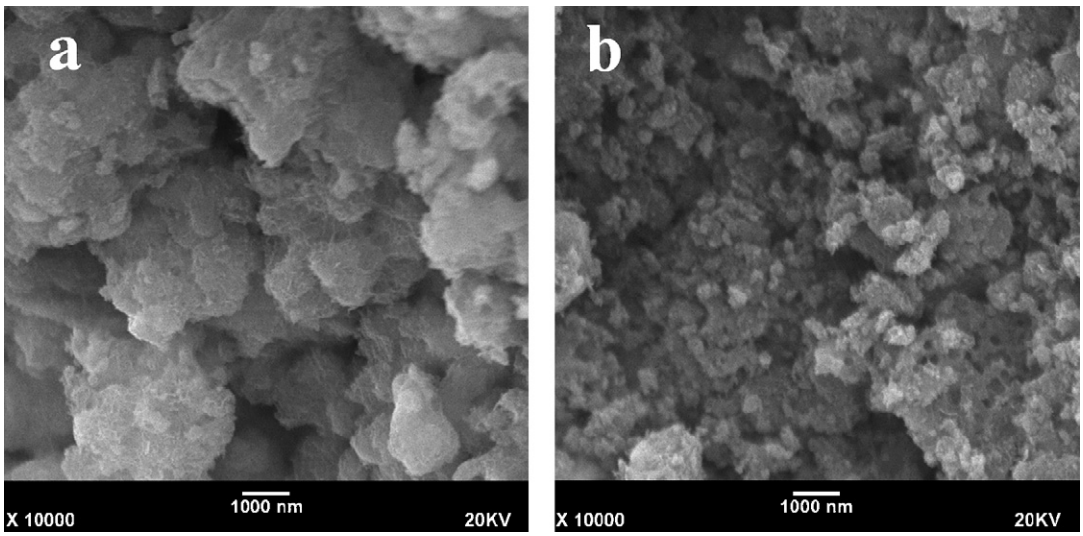

Fig. 3. SEM images of support samples. (a) Al_2O_3 and (b) AZ15.

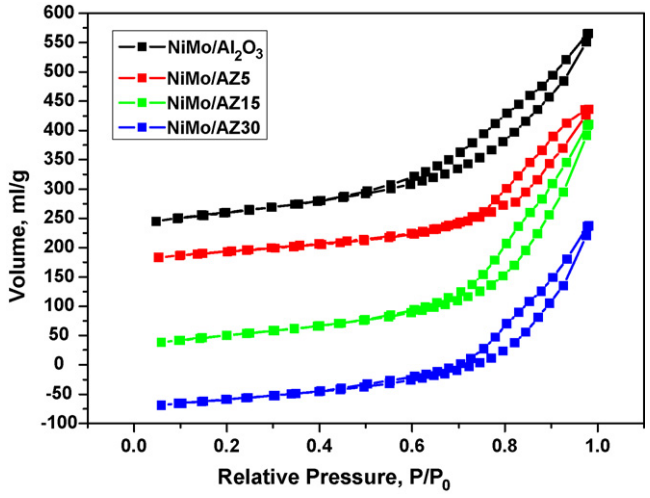

Fig. 4. The nitrogen adsorption/desorption isotherms of NiMo/AZ*x* catalysts.

common mesoporous solids (2–50 nm) [23]. According to IUPAC classification, the hysteresis loops of all NiMo/AZ*x* were close to type H2. This indicated the presence of a significant amount of secondary mesopores. From Table 2, it can be seen that the addition of ZrO_2 into support caused a reduction in the surface area, but an increase in the average pore diameters. This phenomenon might be derived from the two respective reasons. One was the ZrO_2 particles deposited in the pores of Al_2O_3 and blocked part of the small pores. The other was the morphology of composite supports changed from big blocks into small particles (observed from SEM image) which formed more interpores between the particles.

Table 2
Textural properties of NiMo/AZ*x* catalysts.

Samples	BET surface area ($m^2\ g^{-1}$)	Pore volume ($cm^3\ g^{-1}$)	Average diameter (nm)
$NiMo/Al_2O_3$	216.4	0.56	10.5
NiMo/AZ5	156.4	0.44	11.3
NIMo/AZ15	183.8	0.64	13.8
NiMo/AZ30	150.6	0.52	13.9

The pore diameter distribution curves of the samples are shown in Fig. 5. It could be seen that, compared with the $NiMo/Al_2O_3$ catalyst, the volumes of small pores (diameter ranging from 2 to 5.7 nm) of NiMo/AZ*x* samples were reduced remarkably, this could explain the reason of the increasing of the average pore diameter as ZrO_2 was incorporated into the support. In addition, the NiMo/AZ15 had the maximum of pore diameter distribution of 9.1 nm and the highest pore volume compared with the others. It would provide more efficient surface area and pore volume for the catalytic reaction.

3.4. H_2-TPR

To investigate the interaction between the composite supports and the active metals, the corresponding H_2-TPR measurements were carried out and the results are illustrated in Fig. 6. The TPR profiles of all the samples exhibited two main reduction peaks centered at about 380–400 and 770–800 °C. The low temperature peak (380–400 °C) was generally associated to the reduction of Mo^{6+} to Mo^{4+} of polymeric octahedral Mo species that weakly bonded to the composite supports, and the peak at about 770–800 °C in the samples comprised the deep reduction of all Mo species, including highly dispersed tetrahedral Mo species and

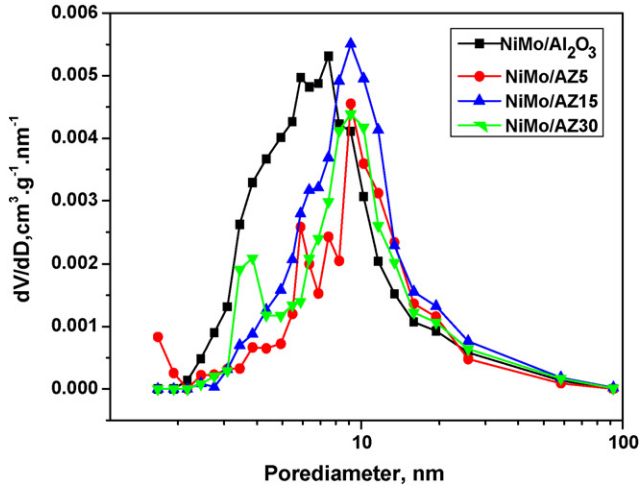

Fig. 5. The pore size distributions of NiMo/AZ*x* catalysts.

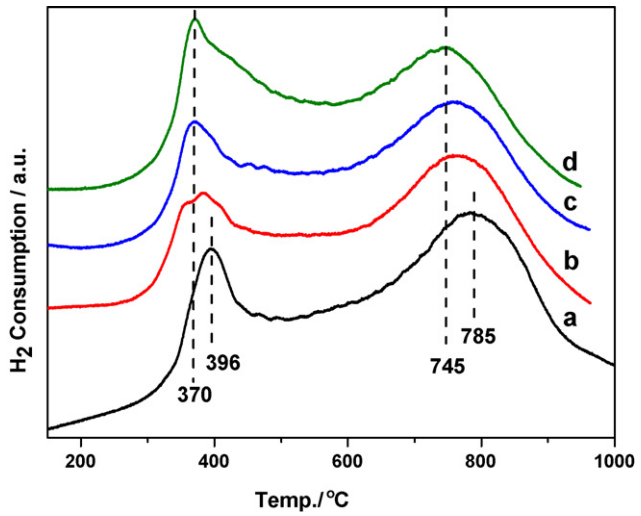

Fig. 6. The H_2-TPR profiles of the oxide NiMo/AZ*x* catalysts. (a) $NiMoAl_2O_3$, (b) NiMo/AZ5, (c) NiMo/AZ15, and (d) NiMo/AZ30.

the second step of reduction of the polymeric octahedral Mo species from Mo^{4+} to Mo^0 [24,25]. It could be seen that the TPR patterns changed with the increasing of the ZrO_2 contents in the samples. Both the first and the second peaks shifted to lower temperature, indicating that the incorporation of ZrO_2 into supports resulted in the easier reduction of the catalysts. The relative integral areas of the second peak decreased with the increasing ZrO_2 contents in the samples. This suggested that the incorporation of ZrO_2 into supports decreased the interaction between the active metal and the composite supports, and it leaded to form some other Mo species which are easier to be reduced. This result was further confirmed by the UV–vis DRS spectra. Moreover, compared with the $NiMo/Al_2O_3$, the NiMo/AZ*x* catalysts showed one broad peak at ~380 °C, especially for the NiMo/AZ30. In addition, no peak was observed in the temperature range of 600–630 °C in all the samples, which was attributed to the reduction of bulk MoO_3 [24]. Theses results were in accordance with those of XRD results.

The TPR studies of NiMo/AZ15 catalysts in which the supports were calcined at different temperatures were also carried out. The results are shown in Fig. 7. From Fig. 7, it can be seen that the intensities of the first peak increased sharply with the support

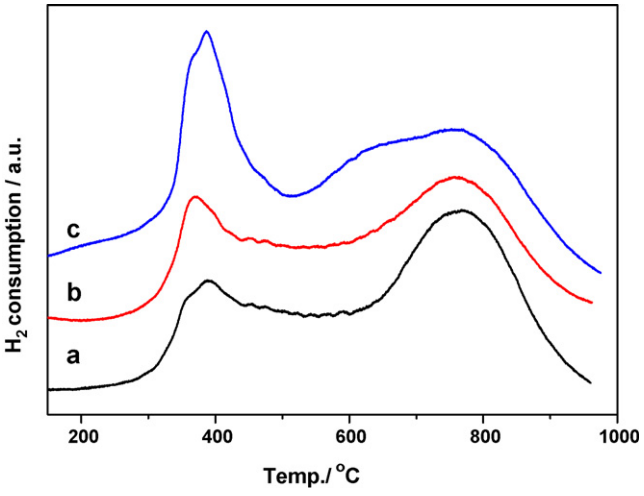

Fig. 7. The H_2-TPR profiles of the oxide NiMo/AZ15 catalysts in which the supports were calcined at (a) 400 °C, (b) 550 °C, and (c) 800 °C.

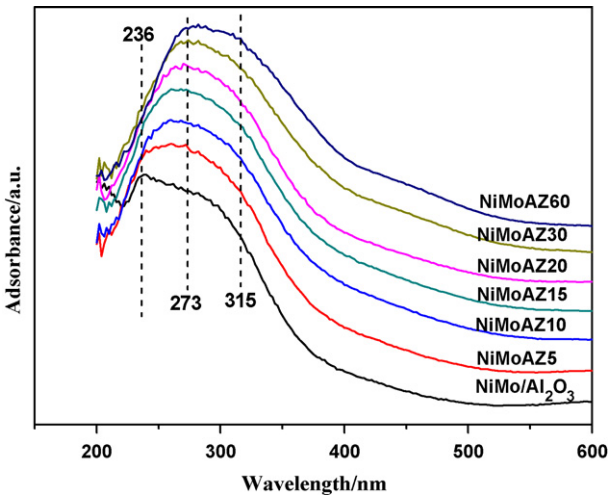

Fig. 8. UV–vis DRS spectra of NiMo/AZ*x* catalysts.

calcined temperatures increased from 400 to 800 °C. However, the second peak decreased. In addition, a broadened peak was observed in the temperature range of 600–630 °C in the sample whose support was calcined at 800 °C. This is attributed to the reduction of bulk MoO_3 [24]. The results suggested that the support calcined at relatively high temperature was favorable for producing the polymeric MoO_X species, which might because the high temperature promoted the formation of more stable structure of composites. Thus, the Mo species would be easier to form the polymeric octahedral species or bulk phase with weak interaction with the composite supports.

3.5. UV–vis DRS analysis

The UV–vis DRS spectra of NiMo/AZ*x* series of catalysts are shown in Fig. 8. The spectra were obtained based on the background deductions of the corresponding supports. Since Mo^{6+} has a d^0 electronic configuration, the absorption due to the ligand-to-metal charge transfer (LMCT) transition, O^{2-} to Mo^{6+}, was observed in the range of 200–400 nm. And the absorption bands centered at 230, 250–280 and 250–295, 300–320 nm [26–29] were assigned to the isolated molybdate (tetrahedral) and polymolybdate (octahedral) species, respectively. The DRS spectra of NiMo/AZ*x* catalysts in Fig. 8 showed that those two types of species (tetrahedral and octahedral) of Mo^{6+} ions were present in all the samples. However, compared with the NiMo/AZ*x* catalysts, the $NiMo/Al_2O_3$ had an obvious absorption band centered at around 236 nm which was attributed to the isolated molybdate (tetrahedral) [27], and the absorption band shifted from 230–280 to 270–330 nm with ZrO_2 content increasing. So it was suggested that the content of octahedral coordination Mo^{6+} species increased and that of the isolated molybdate (tetrahedral) decreased. It also indicated that the interactions between supports and MoO_3 were decreased by the introduction of ZrO_2 into the supports, so the catalyst formed more polymolybdate (octahedral) Mo species which was favorable for the formation of the HDS active sites. This was in accordance with the TPR results.

3.6. Pyridine-adsorbed FT-IR analysis

The acidity of NiMo/AZ*x* samples was investigated by pyridine-adsorbed FT-IR method. As it can be seen in Fig. 9, IR bands at 1450 and 1540 cm^{-1} were observed, due to the characteristic bands of pyridine chemisorbed on L and B acid sites, respectively. IR band appearing at 1490 cm^{-1} was attributed to pyridine co-adsorbed on both B and L acid sites [30,31]. The results demonstrated that both

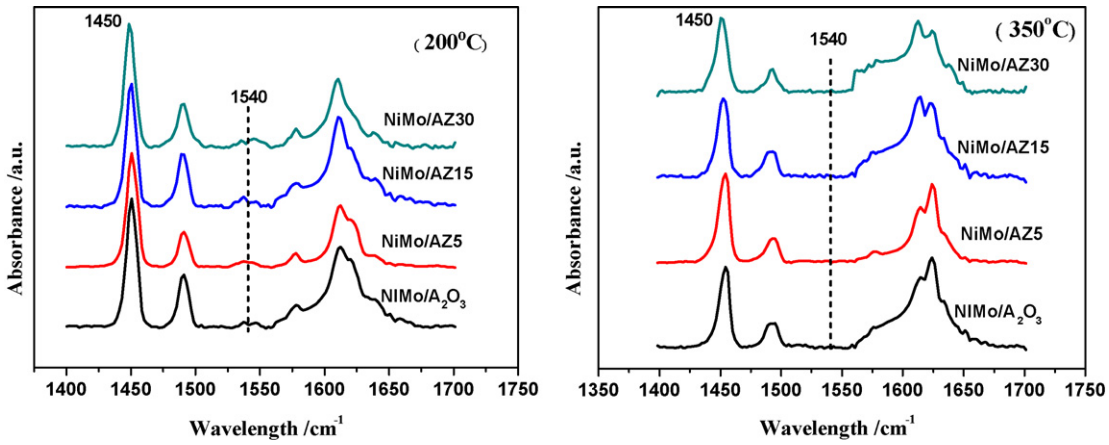

Fig. 9. FT-IR spectra of pyridine adsorption on oxide NiMo/AZ*x* catalysts (degassed at 200 and 350 °C).

Table 3
Amounts of B and L acid sites determined by FT-IR pyridine adsorptions of NiMo/AZ*x* catalysts.

Samples	ZrO_2 m%	Amount of acid sites (μmol g^{-1})				Amount of acid sites (μmol g^{-1})			
		B	L	(B + L)	B/L	B	L	(B + L)	B/L
NiMo/Al_2O_3	0	22.02	42.82	64.84	0.51	–	111.67	111.67	–
NiMo/AZ5	10	25.38	329.50	354.88	0.08	15.24	121.94	137.18	0.12
NiMo/AZ15	15	42.33	363.21	405.54	0.12	–	108.13	108.13	–
NiMo/AZ30	30	33.86	361.17	395.03	0.09	–	102.13	102.13	–

B and L acid sites co-existed on NiMo/AZ*x* samples. When the temperature rose from 200 to 350 °C, the IR bands at 1450 and 1490 cm^{-1} could be still detected, but the band at 1540 cm^{-1} disappeared. These results demonstrated that there were scarcely strong B acid sites in the samples.

The acid distributions of NiMo/AZ*x* catalysts were estimated according to the IR spectra, and the data are summarized in Table 3. As can be seen in Table 3, the incorporation of ZrO_2 into supports had an apparent effect on the acidic properties. For the weak acid site (200 °C), the amounts of Lewis acid site increased dramatically as a small amount of ZrO_2 was incorporated into supports. However, the B acid site slightly increased. These led to the great increasing of the total amount of weak acid site, and the decreasing of B_{200}/L_{200} values. But both of L and B acids sites did not increase with the further increasing of the ZrO_2 contents. On the other hand, at the higher degassing temperature (350 °C), only for the NiMo/AZ5 sample was detected a little amount of B acid sites. For the other samples the B acid site was not detected at all. The L acid at 350 °C was changed slightly as the ZrO_2 contents increased. From the above results, it could be found that the incorporation of ZrO_2 into supports had a large effect on the amounts and the distribution of weak acidic site, especially resulted in the large increase of the total amounts of weak L acid site. This might be due to the interaction between the ZrO_2 and Al_2O_3, which led to the excess of the positive or negative charges in the composite oxide structures.

3.7. Catalytic activity

In the present study, the catalytic activities of sulfided NiMo/AZ*x* catalysts were examined in the hydrodenitrogenation (HDN) and hydrodesulfurization (HDS) efficiencies of Daqing FCC diesel oil. The results are shown in Fig. 10. From the data in Fig. 10, it could be observed that the HDS conversions of diesel on the NiMo/AZ*x* series of catalysts exhibited an increasing trend at first and then decreased with the further increasing of ZrO_2 contents. The NiMo/AZ15 gave the highest catalytic activity. In addition, the NiMo/AZ5, NiMo/AZ10 and NiMo/AZ15 catalysts all exhibited higher catalytic activities than NiMo/Al_2O_3 catalyst. This suggested that the introduction of suitable amounts of ZrO_2 into supports could enhance the HDS performances of NiMo catalysts. From the physico-chemical characterization of the NiMo/AZ*x* catalysts, it was obvious that the higher catalytic performances of suitable ZrO_2 contents might be caused by the following two reasons: (i) to reduce the interaction between Al_2O_3 support and the active metal, and led to the formation of the easily reduced Mo species, which formed more active sites in sulfured catalysts and (ii) to enhance the hydrogenation ability of the catalysts [26], which might be attributed to the dramatically increasing of the total amount of acid sites, especially for the L acid sites that played an important role in the hydrogenation process [9,32].

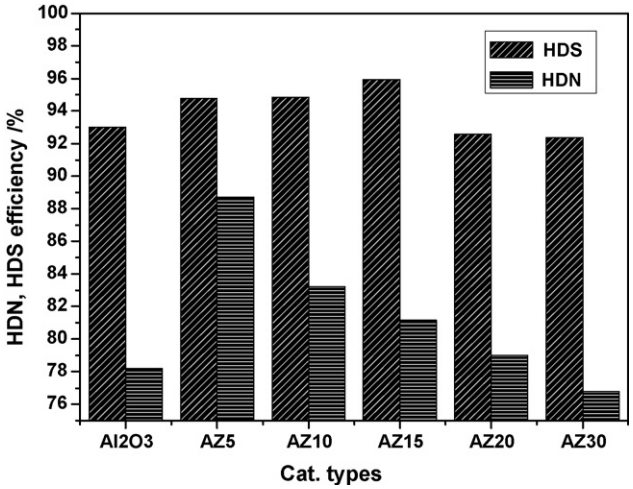

Fig. 10. Diesel HDS and HDN activities of sulfided NiMo/AZ*x* catalysts as a function of ZrO_2 contents in the composite supports.

It could also be seen from Fig. 10 that the HDN efficiencies showed the similar trends to HDS results, but the highest HDN conversion was obtained over the NiMo/AZ5 catalyst, which had a smaller surface area and smallest pore volume (based on the results of the N_2 adsorption). This might be due to the existence of the strong B acid site on its surface according to the pyridine-adsorbed FT-IR results (in Table 3). Since the large amounts of Lewis acid led to the saturation of the aromatic rings and then the C–N bond was easier to be cleaved on the strong B acid site [33]. So it could be drawn a conclusion that during the hydrotreating process, the L and B acid had a cooperative effect, and the strong acid site, especially the strong B acid might play an important role in the HDN process [33].

4. Conclusions

A series of Al_2O_3–ZrO_2 composite oxides were prepared by chemical precipitation method in this study. After calcined at 550 °C, composite oxides presented as amorphous phase in the samples with ZrO_2 contents below 30%. When the ZrO_2 contents increased to 60%, it existed as the tetragonal phase. However, the pure ZrO_2 mainly presented as the monoclinic phase with a little tetragonal phase. Compared with Al_2O_3, the composite oxides exhibited different surface morphologies, and possessed relatively low surface area and higher average pore diameters.

The characterization results of XRD, H_2-TPR and DRS confirmed that the incorporation of ZrO_2 into Al_2O_3 support could improve the dispersion of oxidized Mo species and adjusted the interaction between support and active metal, thus improved the reducibility of molybdenum oxides on Al_2O_3–ZrO_2 supports. The results of pyridine-adsorbed FT-IR verified that NiMo/Al_2O_3–ZrO_2 catalysts possessed more L acid sites than NiMo/Al_2O_3 catalyst, which contributed in some extent to the better HDS and HDN performances than NiMo/Al_2O_3.

The HDS efficiencies of catalysts increased with ZrO_2 contents and kept at high levels compared with the NiMo/Al_2O_3 sample, and reached a maximum at ZrO_2/(ZrO_2 + Al_2O_3) ratio of 15%, which was consistent with its textural properties and the large amounts of Lewis acid sites. The highest HDN efficiency was obtained over NiMo/Al_2O_3–ZrO_2 with the ZrO_2 content of 5%.

Acknowledgements

The authors acknowledge the financial supports from 973 NBRP of China (No. 2004CB217806), and National Natural Science Foundation of China (Nos. 20876173, 20773163 and 20833011).

References

[1] A. Duan, G. Wan, Z. Zhao, C. Xu, Y. Zheng, Y. Zhang, T. Dou, X. Bao, K. Chung, Catal. Today 119 (2007) 13.
[2] T.C. Ho, Catal. Today 98 (2004) 3.
[3] X. Carrier, J.F. Lambert, M. Che, J. Am. Chem. Soc. 119 (1997) 10137.
[4] Y. Okamoto, M. Breysse, G. Murali Dhar, C. Song, Catal. Today 86 (2003) 1.
[5] G.M. Dhar, B.N. Srinivas, M.S. Rana, M. Kumar, S.K. Maity, Catal. Today 86 (2003) 45.
[6] J. Escobar, M.C. Barrera, J.A. de los Reyes, J.A. Toledo, V. Santes, J.A. Colin, J. Mol. Catal. A 287 (2008) 33.
[7] Y. Saih, M. Nagata, T. Funamoto, Y. Masuyama, K. Segawa, Appl. Catal. A: Gen. 295 (2005) 11.
[8] W. Huang, A. Duan, Z. Zhao, G. Wan, G. Jiang, T. Dou, K.H. Chung, J. Liu, Catal. Today 131 (2008) 314.
[9] S. Damyanova, L. Petrov, M.A. Centeno, P. Grange, Appl. Catal. A: Gen. 224 (2002) 271.
[10] J.R. Grzechowiak, J. Rynkowski, I. Wereszczako-Zielinska, Catal. Today 65 (2001) 225.
[11] C. Pophal, F. Kameda, K. Hoshino, S. Yoshinaka, K. Segawa, Catal. Today 39 (1997) 21.
[12] A.A. Cecílio, S.H. Pulcinelli, C.V. Santilli, Y. Maniette, V.T. da Silva, J. Sol–Gel Sci. Technol. 31 (2004) 87.
[13] W. Zhaobin, X. Qing, G. Xinxuan, Appl. Catal. 63 (1990) 305.
[14] S. Damyanova, P. Grange, B. Delmon, J. Catal. 168 (1997) 421.
[15] V. Quaschning, J. Deutsch, P. Druska, H.J. Niclas, E. Kemnitz, J. Catal. 177 (1998) 164.
[16] G. Li, W. Li, M. Zhang, K. Tao, Catal. Today 93–95 (2004) 595.
[17] G. Li, W. Li, M. Zhang, K. Tao, Appl. Catal. A: Gen. 273 (2004) 233.
[18] S.K. Maity, J. Ancheyta, L. Soberanis, F. Alonso, M.E. Llanos, Appl. Catal. A: Gen. 244 (2003) 141.
[19] Z.B. Wei, W. Yan, H. Zhang, T. Ren, Q. Xin, Z. Li, Appl. Catal. A: Gen. 167 (1998) 39.
[20] Y. Zhao, B. Shen, W. Zhang, R. Tian, Z. Zhang, J. Gao, Fuel 87 (2008) 2343.
[21] T. Klimova, M.L. Rojas, P. Castillo, R. Cuevas, J. Ramirez, Micropor. Mesopor. Mater. 20 (1998) 293.
[22] R.C. Garvie, J. Phys. Chem. 69 (1965) 1238.
[23] J. Rouquerol, D. Avnir, C.W. Fairbridge, Pure Appl. Chem. 66 (1994) 1739.
[24] R. Lopez Cordero, F.J. Gil Llambias, A. Lopez Agudo, Appl. Catal. 74 (1991) 125.
[25] R. Lopez Cordero, A. Lopez Agudo, Appl. Catal. A: Gen. 202 (2000) 23.
[26] O.Y. Gutierrez, G.A. Fuentes, C. Salcedo, T. Klimova, Catal. Today 116 (2006) 485.
[27] J.M. Herrera, J. Reyes, P. Roquero, T. Klimova, Micropor. Mesopor. Mater. 83 (2005) 283.
[28] R.S. Weber, J. Catal. 151 (1995) 470.
[29] G. Xiong, C. Li, Z. Feng, P. Ying, Q. Xin, J. Liu, J. Catal. 186 (1999) 234.
[30] T.R. Hughes, H.M. White, J. Phys. Chem. 71 (1967) 2192.
[31] X. Zhang, J. Wang, J. Zhong, A. Liu, J. Gao, Micropor. Mesopor. Mater. 108 (2008) 13.
[32] O.Y. Gutierrez, D. Valencia, G.A. Fuentes, T. Klimova, J. Catal. 249 (2007) 140.
[33] R. Prins, M. Jian, M. Flechsenhar, Polyhedron 16 (1997) 3235.